Supporting Information

Micropores-induced high-performance Fe–N_x/C electrocatalysts towards the oxygen reduction reaction

Micropores-induced high-performance Fe–N_x/C electrocatalysts towards the oxygen reduction reaction

Yeshen Qin[1,2], Feng Wang[2], De Cheng[1], Lei Feng[1], Chen Wen[1 *], Jiaqiang Zhang[1], Sizhen Li[1], Nan Wang, Jingying Bai[1 *]

[a.] Beijing Spacecrafts Manufacturing Co., Ltd , China Academy of Space Technology, Beijing, 100190, P. R. China.

[b.] State Key Laboratory of Chemical Resource Engineering, Beijing Key Laboratory of Electrochemical Process and Technology for Materials, Beijing University of Chemical Technology, Beijing 100029, P. R. China.

Corresponding Author: Chen Wen,13552907280@163.com,

Jingying Bai, baijy1213@163.com

1. Experimental

Materials

Hydrochloric acid (HCl), isopropanol, ethanol, methanol and tetrahydrofuran (THF) were purchased from Sinopharm. High purity argon, oxygen and nitrogen gas were bought from Beijing AP BAIF Gases Industry Co. Ltd. Iron (II) phthalocyanine (FePc), commercial Pt/C (20 wt.%), Nafion solution (5 wt.%) were purchased from TCI, Johnson Matthey and DuPont, respectively. Commercial carbon black (Vulcan), and high specific surface area microporous carbon (MC) were purchased from Cabot, and Shaanxi Coal and Chemical Industry Group Co., Ltd respectively. Ultrapure water (18.2 MΩ cm) obtained from a water purification system (TTL-6B) without further purity.

Characterization and electrochemical testing

Powder X-ray diffraction (XRD) patterns were profiled on an X-ray diffractometer (D/max-2500, Rigaku, Japan) with Cu Kα radiation (λ = 1.54056 Å) source. Scanning electron microscopy (SEM) and high-resolution transmission electron microscopy (HR-TEM) images were taken on the FE-JSM-6701F (JEOL, Japan) and JSM-2100 (JEOL, Japan) microscopes, respectively. The Brunauer-Emmett-Teller (BET) specific surface area and pore size distribution were determined by nitrogen adsorption-desorption measurements with a Quantachrome AUTOSORB-SI instrument. Raman spectra were recorded with a Horiba Jobin Yvon LabRam HR800 confocal microscope using a laser of 632.8 nm. The X-ray photoelectron spectroscopy (XPS) was performed with the Thermo Fisher Scientific ESCALAB 250 spectrometer using the C 1s peak (285 eV) as the reference for binding energy calibration. The FT-IR analysis was performed to determine the functional groups using Nicolet

8700/Continuum XL and the ultraviolet (UV) absorption spectroscopy was carried out using a Shimadzu UV-2450 with wavelength from 300 to 900 nm.

All the electrochemical measurements were conducted with an RRDE-3A electrochemical workstation (ALS/DY2323 Bi-potentiostat) using a standard three-electrode system at room temperature. A glassy carbon rotating disk electrode (RDE) or rotating ring disk electrode (RRDE) coated with electrocatalyst was used as the working electrode, a Pt wire and a saturated calomel electrode as the counter and reference electrodes, respectively. All potentials reported in this work were in reference to the reversible hydrogen electrode (RHE). In a typical preparation of working electrode, 10 mg of electrocatalyst was ultrasonically blending with 2.0 mL of ethanol and 20 μL of Nafion (5 wt. %, Dupont) for 0.5 h to form a homogeneous electrocatalyst ink, 10 μL of which was transferred onto the polished RDE or RRDE, leading to a geometric loading of 0.394 mg cm^{-2}. The commercial Pt/C (20 wt. % of Pt, Johnson Matthey) working electrode was also used as a reference with the Pt loading of 20 μg cm^{-2}.

All the potentials were calibrated to the potentials *vs.* RHE (Potentials *vs.* RHE = potential *vs.* SCE + 0.241+0.0591*pH V). The ORR experiments were carried out in 0.1 M KOH solution at the ambient temperature after being purged with O_2 or N_2 gas for 20 min. The glassy carbon rotating disk electrode is 4 mm in diameter. Koutecky–Levich (K-L) plots reflecting the relation of current density (J^{-1}) versus rotation rate ($\omega^{-1/2}$) were constructed according to:

$$J^{-1} = J_k^{-1} + (0.2nFC_{O_2}D_{O_2}^{2/3}\gamma^{-1/6})^{-1}\omega^{-1/2}$$

where J_k is the kinetic-limiting current, n is the number of electrons transferred per oxygen molecule, F is the Faraday constant (96,485 C mol^{-1}), C_{O2}, D_{O2} and γ are the concentration, the diffusion coefficient of oxygen and the kinematic viscosity, respectively, in 0.1 M KOH.

For the Tafel plots, the kinetic current (J_k) was calculated from the mass-transport correction of RDE by:

$$J_k = \frac{J \times J_d}{J_d - J}$$

where J_d is the diffusion limited current density.

The percentage of hydrogen peroxide yield ($\% \, HO_2^-$) and the corresponding electron transfer number (n) was calculated by RRDE data from:

$$\% \, HO_2^- = 200 \times \frac{I_r/N}{I_d + I_r/N}$$

$$n = 4 \times \frac{I_d}{I_d + I_r/N}$$

where I_d is disk current, I_r is ring current and $N = 0.37$ is the current collection efficiency of the Pt ring.

2. Supporting Results and Discussion.

Table S1. Pore characteristics of MC, Fe–N–MC, CB, Fe–N–CB, CNT, and Fe–N–CNT.

sample	S_{BET} (m^2 g^{-1})	S_{micro} (m^2 g^{-1})	Porous volume (m^3 g^{-1})	microporous volume (m^3 g^{-1})
MC	3072	2305	1.613	1.011
Fe–N–MC	812	621	0.406	0.275
CB	230	96	0.207	0.041
Fe–N–CB	65	0	0.107	0
CNT	22	0	0.030	0
Fe–N–CNT	21	0	0.027	0

Table S2. The C-, N-, O- and Fe-content of Fe–N–MC, Fe–N–CB and Fe–N–CNT.

Sample	C (at. %)	N (at. %)	Content of different N species (at. %)		O (at. %)	Fe (at. %)	Content of different Fe species (at. %)	
			Pyrrole N /M-N	C-N			Fe (Ⅱ)	Fe (Ⅲ)
Fe–N–MC	83.51	4.41-	2.33	2.08	10.83	1.25	0.42	0.83
Fe–N–CB	85.68	6.37	1.11	5.26	7.34	0.62	0.28	0.34
Fe–N–CNT	86.62	4.03	2.15	1.88	8.86	0.49	0.23	0.26
FePc	81.35	10.92	1.92	9.00	6.28	1.45	1.03	0.42

Table S3. Mössbauer parameters and assignment of the six components featured in the deconvoluted Mössbauer spectrum of Fe–N–MC.

Fe species	IS / mm s^{-1}	QS / mm s^{-1}	Area (%)	assignment
D1	0.34113	0.7324	83.25	$Fe^{II}N_4$
D2	0.61689	2.1965	7.04	$Fe^{II}N_{2+2}$
D3	0.07068	1.8890	9.72	$N-Fe^{(II/III)}-N_{2+2}$

Table S4. The electrochemical performance of Fe–N–MC, Fe–N–CB, Fe–N–CNT and 20% Pt/C in 0.1 M KOH

Sample	**E_{onset} (V*)**	**$E_{1/2}$ (V)**	**J_d @ 0.1 V (mA cm^{-2})**	**J_k @ 0.9 V (mA cm^{-2})**
Fe–N–MC	0.97	0.90	6.16	5.51
Fe–N–CB	0.95	0.86	6.03	1.06
Fe–N–CNT	0.90	0.80	5.75	0.15
Pt/C	0.97	0.84	6.10	1.25

***:** versus reversible hydrogen electrode, *vs.* RHE, the same below

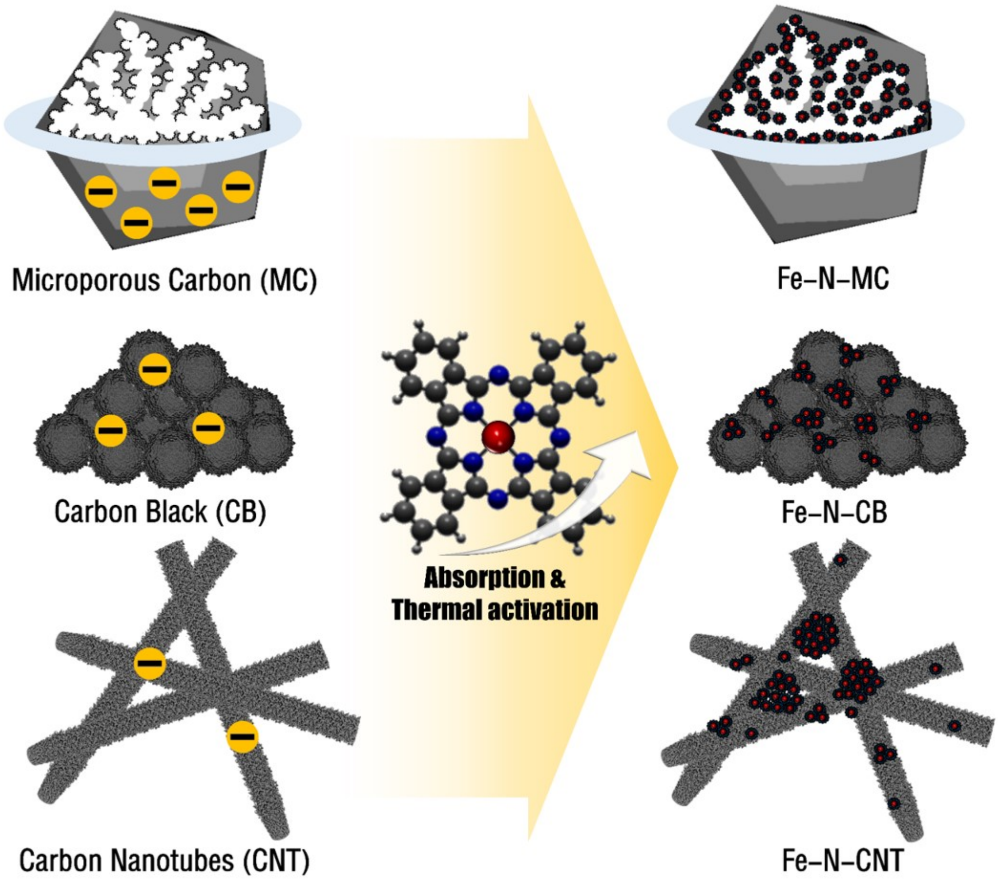

Scheme S1. The preparation process of Fe–N–MC, Fe–N–CB and Fe–N–CNT.

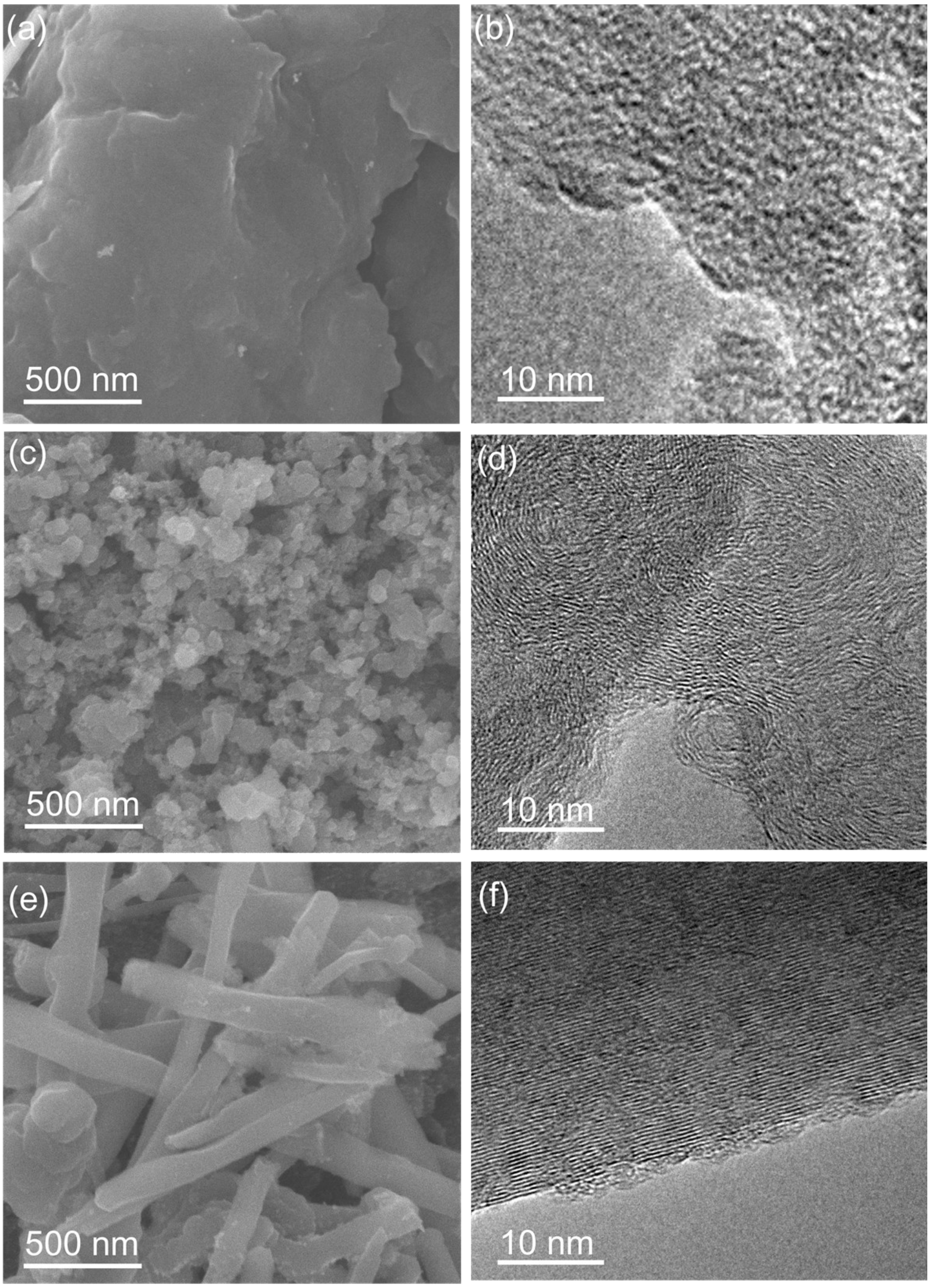

Fig. S1 Typical SEM and corresponding TEM images of (a, b) MC (c, d) CB and (e, f) CNT.

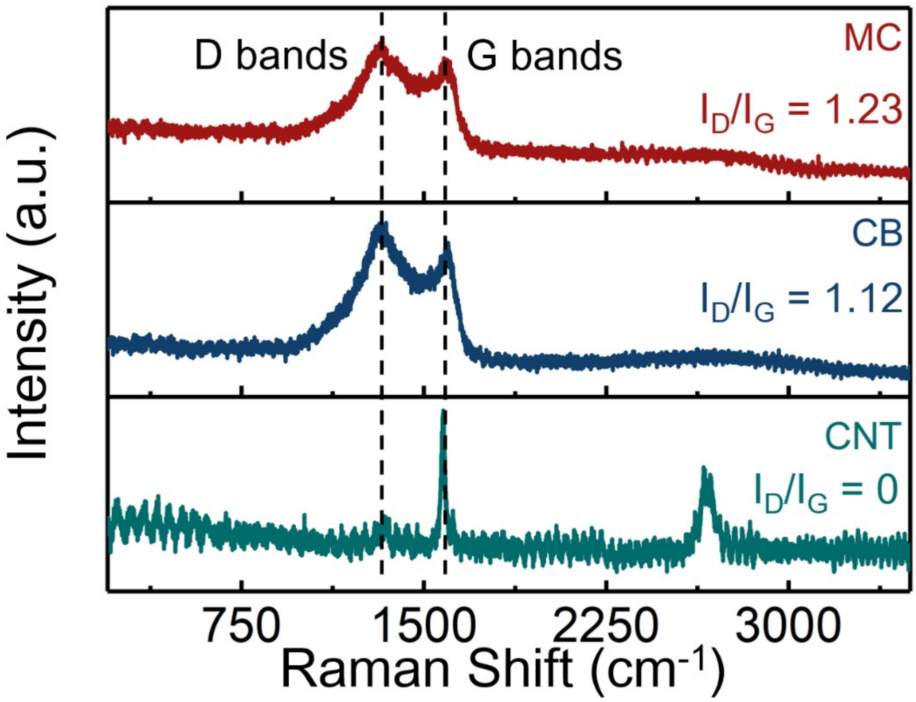

Fig. S2 Raman spectra of MC, CB and CNT carbon supports.

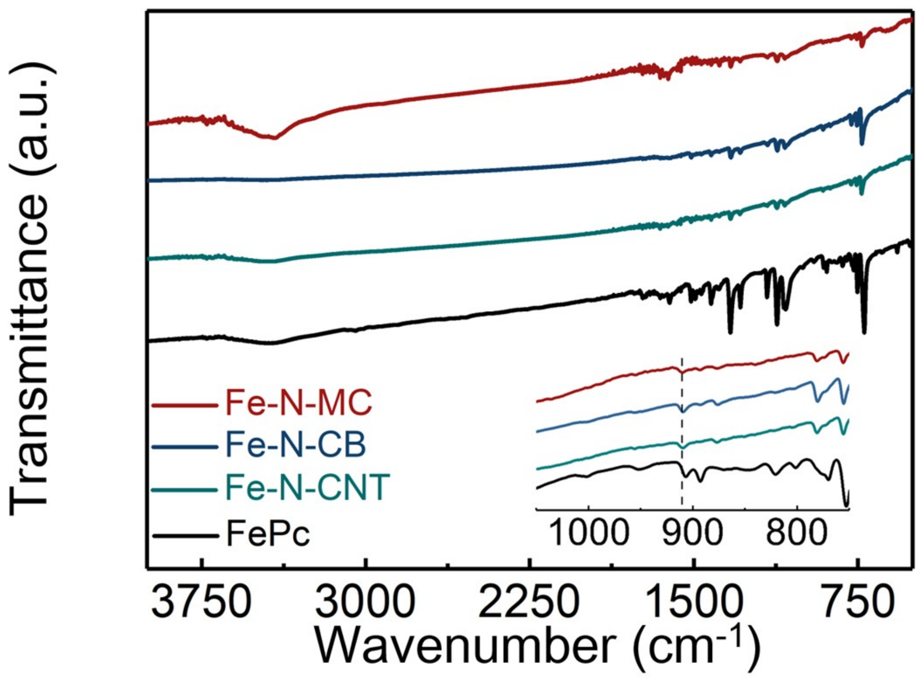

Fig. S3 FT-IR spectra of Fe–N–MC, Fe–N–CB, Fe–N–CNT and FePc supports.

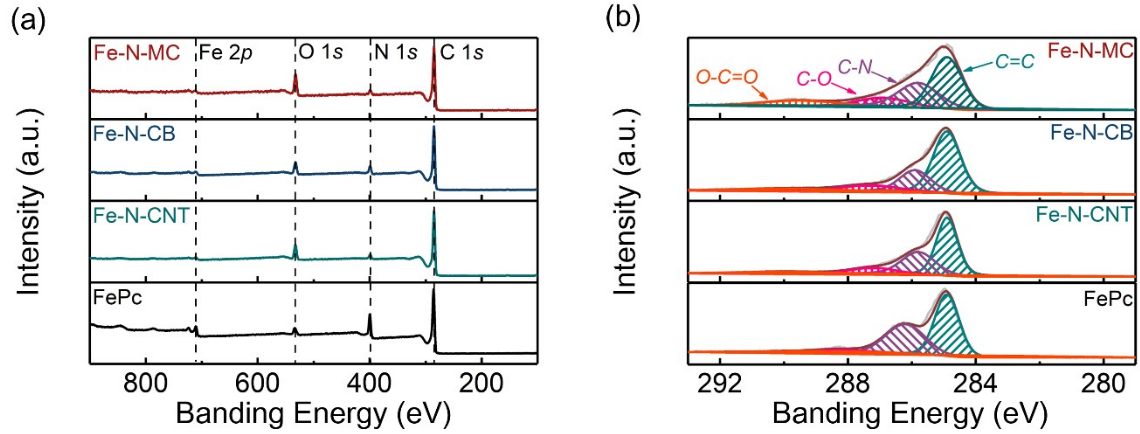

Fig. S4 (a) Survey XPS spectra and (b) High-resolution XPS spectra of C 1s for the Fe–N–MC, Fe–N–CB and Fe–N–CNT electrocatalysts.

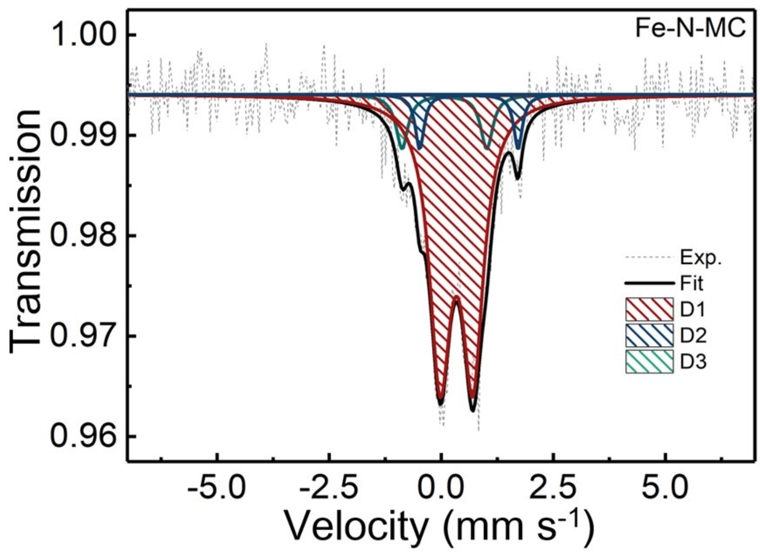

Fig. S5 ^{57}Fe Mössbauer spectroscopy of Fe–N–MC.

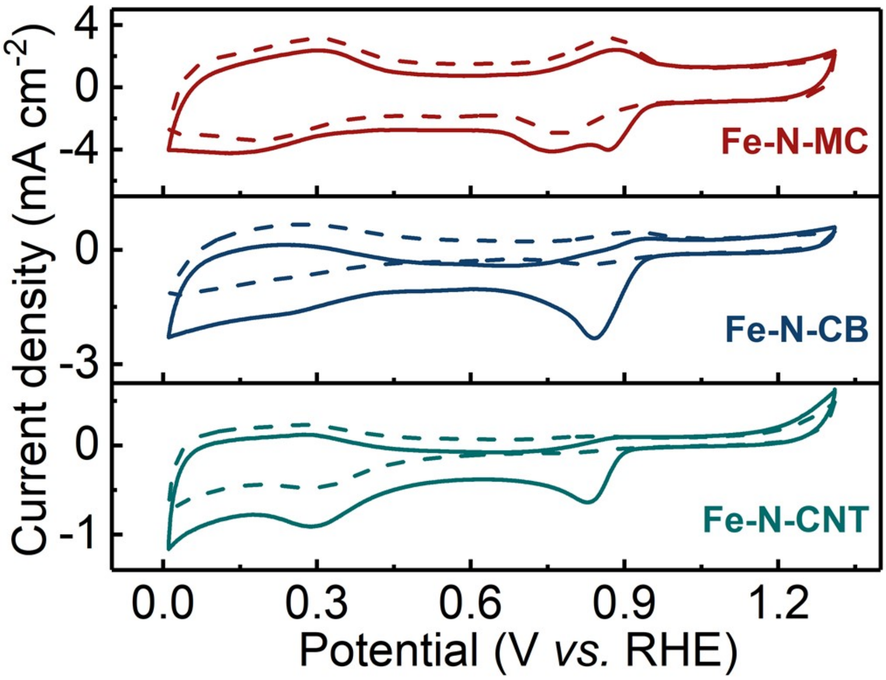

Fig. S6 CV curves for Fe–N–MC, Fe–N–CNT, Fe–N–CB in O_2-saturated (solid line) and N_2-saturated (dash line) 0.1 M KOH solution at a sweep rate of 50 mV s^{-1}.

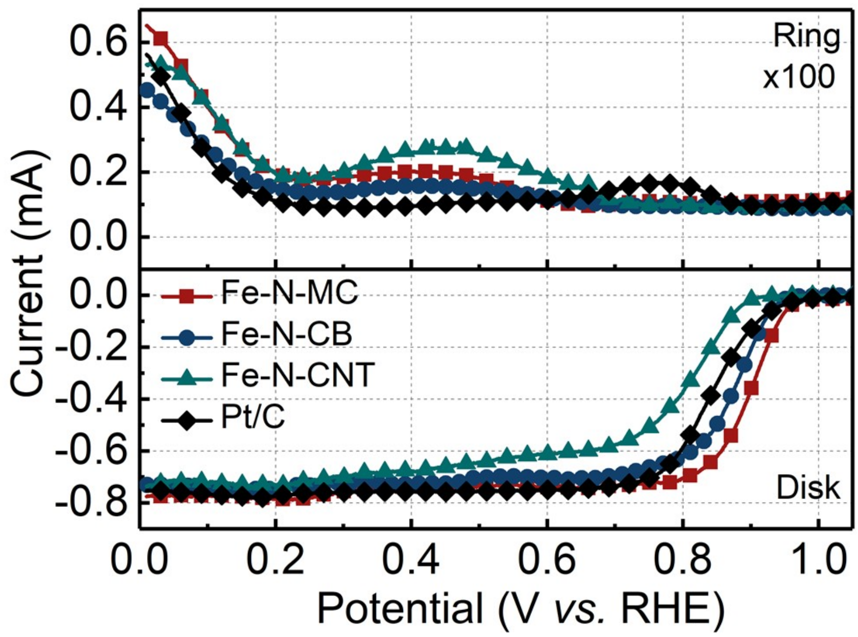

Fig. S7. The disk current (the lower half) and ring current (the upper half) in the RRDE tests of Fe–N–MC, Fe–N–CNT, Fe–N–CB and Pt/C in O_2-saturated 0.1 M KOH solution at a sweep rate of 5 mV s^{-1} with a rotation rate of 1600 rpm.

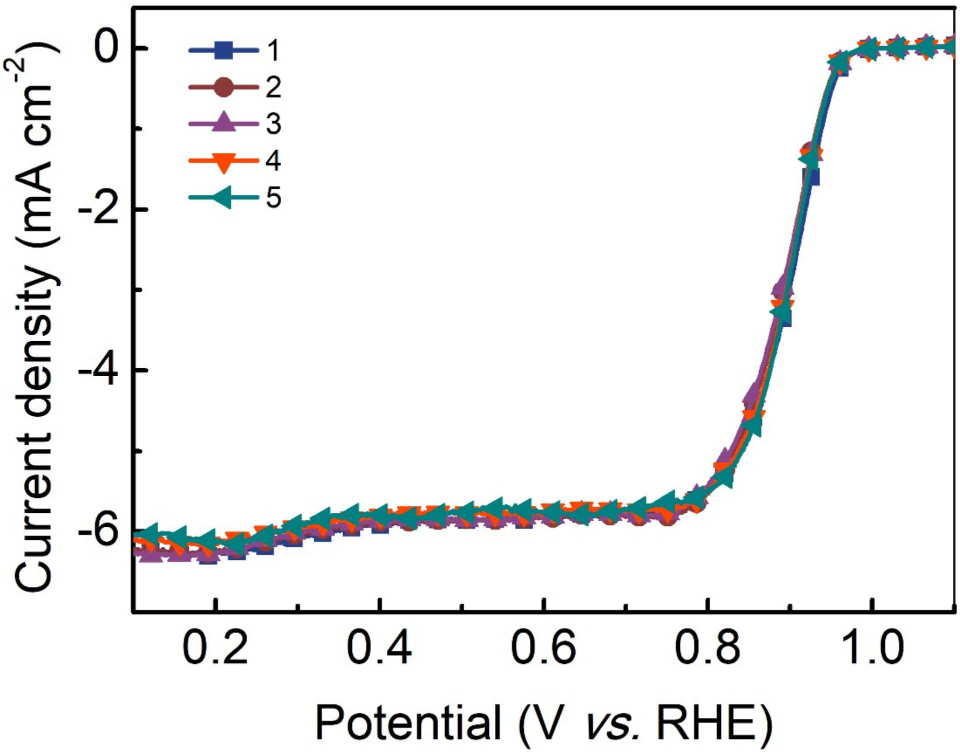

Fig. S8 The ORR performance of Fe–N–MC electrocatalysts which were prepared in large-scale from different areas of crucible.

Table S6. Comparison of ORR performance in alkaline and acidic electrolyte for Fe–N–MC with the reported Fe–N–C (derived from FePc) catalysts.

Sample	**Electrolyte**	**E_{onset} (V)**	**$E_{1/2}$ (V)**	**Ref.**
$FePc/Ti_3C_2T_x$	0.1 M KOH	0.975 *vs.* RHE	0.886 *vs.* RHE	S1
FePc–Py–CNT	0.1 M KOH	0.990 *vs.* RHE	0.915 *vs.* RHE	S2
NT–FePc–400	0.1 M KOH	0.94 *vs.* RHE	0.86 *vs.* RHE	S5
RGO–FePc	0.1 M KOH	0.020 *vs.* Hg/HgO	-0.025 *vs.* Hg/HgO	S6
CNT–FePc	0.1 M KOH	0.018 *vs.* Hg/HgO	-0.024 *vs.* Hg/HgO	
DCI–Fe–700	0.1 M KOH	0.95 *vs.* RHE	0.88 *vs.* RHE	S8
SA–Fe–HPC	0.1 M KOH	0.99 *vs.* RHE	0.89 *vs.* RHE	S9
Fe–N–MC	0.1 M KOH	0.98 *vs.* RHE	0.90 *vs.* RHE	This work

References

S1. Li, Z.; Zhuang, Z.; Lv, F.; Zhu, H.; Zhou, L.; Luo, M.; Zhu, J.; Lang, Z.; Feng, S.; Chen, W.; Mai, L.; Guo, S. The Marriage of the FeN4 Moiety and MXene Boosts Oxygen Reduction Catalysis: Fe 3d Electron Delocalization Matters. *Adv. Mater.* **2018,** *30*, 1803220.

S2. Cao, R.; Thapa, R.; Kim, H.; Xu, X.; Gyu Kim, M.; Li, Q.; Park, N.; Liu, M.; Cho, J. Promotion of oxygen reduction by a bio-inspired tethered iron phthalocyanine carbon nanotube-based catalyst. *Nat. Commun.* **2013,** *4*, 2076.

S3. Li, T.; Peng, Y.; Li, K.; Zhang, R.; Zheng, L.; Xia, D.; Zuo, X. Enhanced activity and stability of binuclear iron (III) phthalocyanine on graphene nanosheets for electrocatalytic oxygen reduction in acid. *J. Power Sources* **2015,** *293*, 511-518.

S4. Li, W.; Yu, A.; Higgins, D. C.; Llanos, B. G.; Chen, Z. Biologically Inspired Highly Durable Iron Phthalocyanine Catalysts for Oxygen Reduction Reaction in Polymer Electrolyte Membrane Fuel Cells. *J. Am. Chem. Soc.* **2010,** *132*, 17056-17058.

S5. González-Gaitán, C.; Ruiz-Rosas, R.; Morallón, E.; Cazorla-Amorós, D. Relevance of the Interaction between the M-Phthalocyanines and Carbon Nanotubes in the Electroactivity toward ORR. *Langmuir* **2017,** *33*, 11945-11955.

S6. Arul, A.; Pak, H.; Moon, K. U.; Christy, M.; Oh, M. Y.; Nahm, K. S. Metallomacrocyclic–carbon complex: A study of bifunctional electrocatalytic activity for oxygen reduction and oxygen evolution reactions and their lithium-oxygen battery applications. *Appl. Catal. B-Environ.* **2018,** *220*, 488-496.

S7. Zhang, Q.; Wang, J.; Yu, P.; Song, F.; Yin, X.; Chen, R.; Nie, H.; Zhang, X.; Yang, W. Porous carbon electrocatalyst with exclusive metal-coordinate active sites for acidic oxygen reduction reaction. *Carbon* **2018,** *132*, 85-94.

S8. Zhang, Z.; Gao, X.; Dou, M.; Ji, J.; Wang, F. Fe–Nx moiety-modified hierarchically porous carbons derived from porphyra for highly effective oxygen reduction reaction. *J. Mater. Chem. A* **2017,** *5*, 1526-1532.

S9. Zhang, Z.; Sun, J.; Wang, F.; Dai, L. Efficient Oxygen Reduction Reaction (ORR) Catalysts Based on Single Iron Atoms Dispersed on a Hierarchically Structured Porous Carbon Framework. *Angew. Chem. Int. Ed.* **2018,** *57*, 9038-9043.